Available online at www.sciencedirect.com
ScienceDirect
Trans. Nonferrous Met. Soc. China 31(2021) 2773−2786
Transactions of Nonferrous Metals Society of China
www.tnmsc.cn

Smart-microstructures of composites for electrical contacts with frameless packing of Cr and W in copper

L. E. BODROVA, S. Yu. MELCHAKOV, A. B. SHUBIN, E. Yu. GOYDA

Institute of Metallurgy of the Ural Branch of the Russian Academy of Sciences, 620016, Ekaterinburg, 101, Amundsen Street, Russian Federation

Received 27 October 2020; accepted 16 April 2021

Abstract: $W_{45}Cu_{55}$, $Cr_{65}Cu_{35}$, and $Cr_{32}W_{14}Cu_{54}$ alloys were obtained in order to study the mechanism of "smart response" of the structure of these alloys when using them as arc-resistant circuit-breakers. These alloys differ from industrial ones with frameless packing of Cr and W phases in the copper matrix. The alloy production method is based on the infiltration of copper melt into a mixture of non-compacted Cr and W powders under vibration exposure (80 Hz). The research results show an increase in the arc resistance of contacts when changing from "frame" packing of W to "frameless," as well as the decisive role of Cr in the processes of self-dispersion of arc-resistant phases and passivation of W and Cu. Based on the obtained results, conclusions are drawn about the advantage of frameless packing of arc-resistant phases in copper and the reasons for the "smart behavior" of the structure of Cr-containing contacts in response to functional loads in the presence of oxygen and an inert atmosphere.

Key words: Cr−W−Cu electro-contact materials; infiltration; smart-structure; self-dispersion

1 Introduction

Different methods are utilized to produce commercial electric contact materials W−Cu and Cr−Cu with a high content of arc-resistant phases, including infiltration of copper melt into a "frame" sintered from refractory powders, mechanical alloying, high-temperature liquid-phase sintering, electric-arc or vacuum induction melting, and casting with rapid cooling [1−4]. One can also note such synthetic techniques as surface alloying, microwave and spark plasma sintering, metal injection molding, high-pressure casting, explosive compact-coating, and infiltration of melt under vibration [5−12].

Today, there is a tendency to expand the use of electrical contact arc-resistant Cr−Cu materials instead of conventional W−Cu despite of higher melting temperature, hardness, and wear resistance of W in comparison with Cr [11,13−16]. Comparative tests of W−Cu and Cr−Cu composites show the advantages of the latter: higher electro-erosion resistance, lower and at the same time more stable contact resistance [1,17].

However, studies of the mechanisms of interaction of copper with W and Cr under the action of an electric arc explaining the high arc resistance of Cr−Cu electrical contacts are very limited. Thus, in Ref. [18], the beginning of the formation of ultradispersed mixtures (Cu)+(Cr) in the Cr−Cu alloy was found already at a temperature of 1300 °C as a result of mechanical activation of the compositions "Cu melt−Cr powder" by low-frequency vibration. It was suggested that the appearance and development of such structures under the action of arc is one reason for the high arc resistance of Cr−Cu alloys. A similar "blurring" of the Cr−Cu interface and the formation of ultradispersed chromium inclusions in the copper

Corresponding author: S. Yu. MELCHAKOV, E-mail: s.yu.melchakov@gmail.com
DOI: 10.1016/S1003-6326(21)65692-3

matrix were found earlier in the Cu−50Cr alloy after irradiation of its surface with a high-current pulsed electron beam at 20 and 30 keV [14]. CHAI et al [14] proposed a scheme for the evolution of chromium grains in copper under the action of high-energy beams. And they associated the formation of spherical microparticles of chromium with the process of liquid-phase separation.

In Ref. [19], the structure of formation−decomposition of the solid solution (W,Cr) in the Cu−10W−10Cr alloy was studied. The alloy was obtained using pre-crystallization vibration treatment of the compositions "Cu melt−a mixture of W and Cr powders" for 10 min at 1300 °C. The decay structure is represented by submicron inclusions of secondary tungsten particles in the secondary (W,Cr) matrix.

On the other hand, to increase the functionality of electrical contacts operating in the air, protection from oxidation is required. For this purpose, oxidation passivators (Cr, Zr, Ti, etc) are introduced into copper alloys. Among them, chromium is of the most interest since it passivates both copper and tungsten. It was shown that the oxidation resistance of binary alloy W−Cr and ternary alloys W−Cr−Me (Me=Y, Ti, Si, Nb) is much higher than that of pure W [20−33]. The adaptive stability of these alloys at high temperatures allowed us to classify them as smart materials.

At elevated temperatures, Cr and W form a continuous series of solid solutions, which decompose on cooling into two solid solutions (W,Cr) ↔ (W) + (Cr) [19,34]. It was also shown that chromium, as a decay product, is an effective passivator of W [20].

Thus, Cr−W−Cu alloys containing arc-resistant components can be a promising material for electrical contacts; however, we have not found any information in the literature about their use.

It is reasonable to assume that temperature increase in Cu−W−Cr alloys when an electric arc is burning will contribute to an increase in both (Cu)+(Cr) ultrafine mixtures and (W,Cr) solid solutions. We suppose that the subsequent cooling of the contact surface when the arc is interrupted should lead to the conservation of ultrafine (Cu)+(Cr) mixtures. Simultaneously, (W,Cr) solid solutions will disintegrate in the Cu−W−Cr system. One should also expect that the multiply repeated cycles of arc burning−interrupting will constantly reproduce such changes in the structure and, thereby slowing down the electric erosion of contacts in operation. Thus, these alloys can exhibit "smart behavior" during operation.

The purpose of this work is to verify and reveal the mechanism of "smart response" of the structure in the alloy with frameless packing of Cr and W phases in copper when using these materials as arc-resistant circuit breakers and also to present an original method of their synthesis.

2 Experimental

2.1 Materials

The research was carried out on model alloys prepared of industrial metal powders without any preliminary treatment. As initial materials, copper (99.98 wt.%) from CJSC Kyshtym Copper Electrolytic Plant, powders of reduced metal chromium (99.6 wt.%) from JSC Polema, and tungsten (99.9 wt.%) from JSC Kirovgrad Hard Alloys Plant were used.

To determine the particle size of chromium and tungsten, the scanning electron microscope (SEM) of type Carl Zeiss Evo 40 was used. The fractional composition of powders was analyzed using the HELOS/BR (Sympatec GmbH) laser diffraction particle analyzer with RODOS/M air dispersion module. The powder morphology and histograms of distribution of particle sizes are shown in Fig. 1.

2.2 Composite alloys production

The alloys were obtained by infiltration of copper melt into the fill of Cr and W uncompacted powders (or their mixtures) under low-frequency vibration using a laboratory apparatus [35]. The apparatus scheme is shown in Fig. 2.

The electromagnetic vibration generator with a capacity of 1.2 kW transmits oscillations with the amplitude of 1 mm and the frequency of 80 Hz through the piston-emitter to the graphite bushing with a set of crucibles of 11 mm in diameter.

Before infiltration, the initial Cr and/or W powders were placed into the graphite crucibles and covered with a copper rod. The graphite bushing with the crucibles was put into the resistance furnace operating area. Activation of the infiltration process was carried out with the application of a low-frequency vibration to the crucibles at 1300 °C

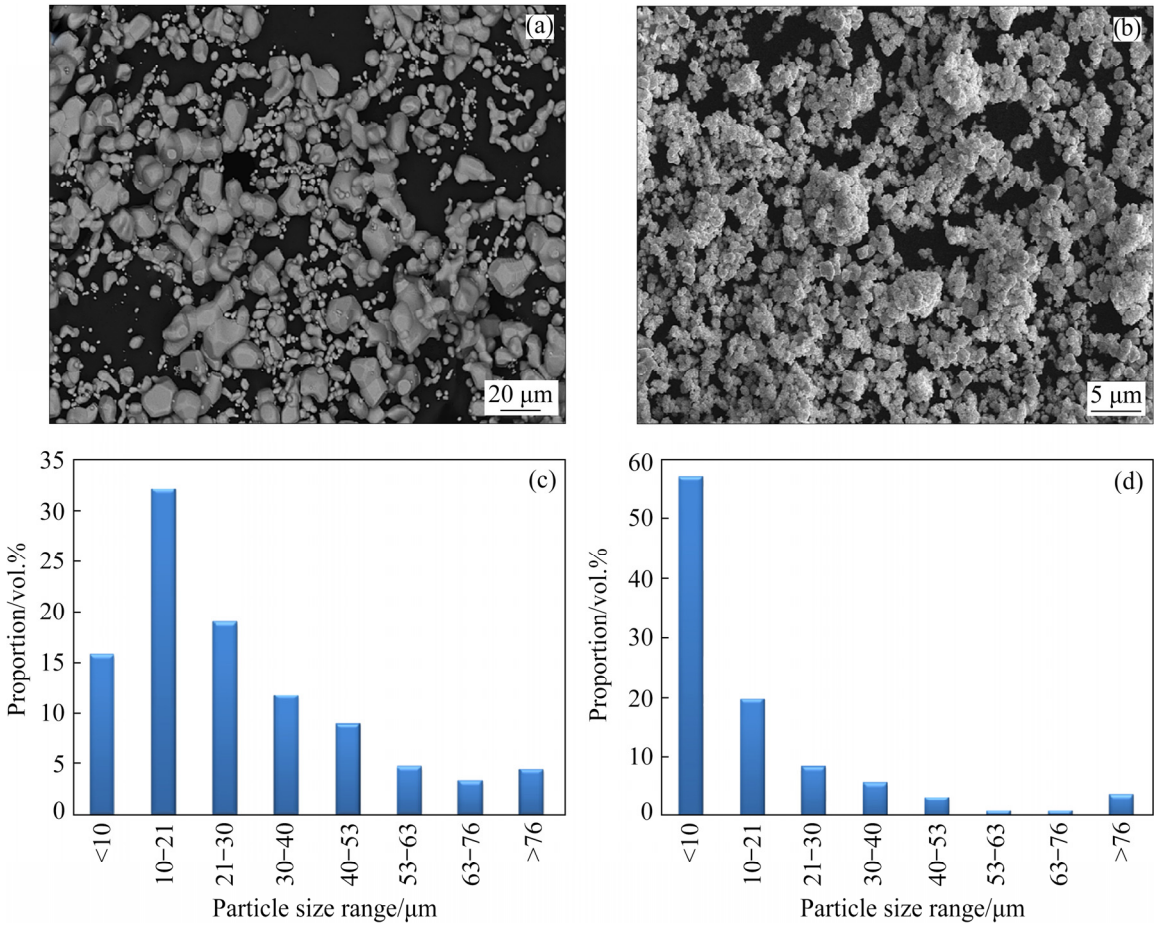

Fig. 1 Powder morphology (a, b) and distribution of particle size (c, d): (a, c) Chromium; (b, d) Tungsten

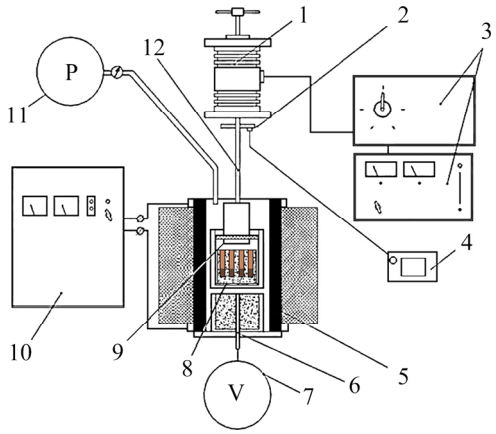

Fig. 2 Scheme of apparatus for low-frequency treatment of "melt−powders" composites: 1−Electromagnetic vibration generator; 2−Acceleration sensor; 3−Vibration generator power unit and control panel; 4−Oscillation frequency meter; 5−Graphite tube-heater; 6−Thermo-couple in sheath; 7−Millivoltmeter; 8−Graphite bushing with cylindrical hollows for initial alloy components (filled); 9−Piston-emitter; 10−Resistance furnace transformer; 11−Balloon with argon; 12−Rod transmitting vibrations to graphite bushing

for 10 min in argon flow. The obtained material was cooled down to 1000 °C with the furnace and then in the air.

The efficiency of the low-frequency vibration impact is based on the mechanical activation of diffusion processes and chemical reactions. In previous investigations, we produced composite alloys with Cu and Al matrices and different refractory inclusions [12,18,19,36−42]. It was shown that the application of low-frequency vibration allows reducing the time of synthesis of alloys with low porosity and specified structure significantly.

2.3 Characterization

The data on the particle size of W powder in our earlier paper [12] do not agree with the results in this study. The particles size in the present work was refined and re-evaluated after additional thorough studies because the powder is prone to cohesion and large and stable agglomerates are formed from small particles.

Electroerosion tests of the obtained alloys were carried out using cylindrical samples (10 mm in diameter and 20 mm in height) on the laboratory device, simulating the work of the AC contactor. The test conditions were as follows: rate of on/off switching of 2 Hz, test current of 125 A, voltage of 50 V, the distance between the contacts of 5 mm, and the total number of arc on/off cycles of 10000.

The alloy microstructure was studied before and after the arc impact test using thin sections obtained perpendicularly to their working surface. The Struers Tegramin-30 sample preparation complex was used to prepare the sections.

Scanning electron microscopes (Carl Zeiss Evo 40, Hitachi TM4000, Tescan Mira 3 LMH, and Phenom-World), as well as the inverted optical metallographic microscope (Olympus GX-51), were used for investigating the alloy structure. X-ray structural analysis was carried out using the XRD-7000 Shimadzu diffractometer in Cu K_α radiation with an adaptor to rotate a thin section in the horizontal plane at 30 r/min.

The hardness of composite layers in the alloys was measured by IT-5010 hardness meter (LLC Test Devices Plant) with the load on indenter (prism) equal to 49.03 N and loading exposure of 15 s. The measurement error of the device was ±1.5%. Vickers microhardness of phases was measured with Buehler Micro Met 5103 using the Image Analysis Program, Thixomet Pro.

3 Results and discussion

Produced alloy ingots have a two-layer constitution with a clear boundary between the layers. The top layer consists of α-copper. The bottom layer is a composite structure of arc-resistant metals nearly uniformly distributing in the copper matrix. The arc-resistant metals do not form a continuous (rigid) frame because they are separated from each other with copper interlayers. Compositions of the obtained alloys are $Cr_{65}Cu_{35}$, $W_{45}Cu_{55}$, and $W_{14}Cr_{32}Cu_{54}$ (in at.%).

When making contacts for the arc-resistance test, the polished surfaces of the ingot bottom parts were used as commuting surfaces. Henceforth, the term “alloy” will only be used for its composite layer.

The vertical cross-sections of the contacts were used to make the alloy microstructure analysis before and after the multiple exposures of the alloy to the electric arc. It was found out that the changes took place only in the top layers of the commuting surfaces. The structure remained unchanged at the depth (i.e., ≥500 μm) of the contacts.

3.1 $Cr_{65}Cu_{35}$ alloy

The images of the $Cr_{65}Cu_{35}$ alloy structure before arc-resistance tests are shown in Fig. 3. It can be seen that the macro distribution of chromium inclusions in the alloy is uniform enough (Fig. 3(a)). The chromium particles mainly preserve their different morphology and wide range of sizes (Figs. 3(b, c)) compared to the initial state (Fig. 1(a)).

The maximum value of the microhardness of large chromium inclusions is not more than 2500 MPa, while in alloys with frame packaging, this limit is 3000 MPa. This is apparently due to the relative softness of the copper sublayer under each chromium grain.

The interphase boundary between chromium particles and α-Cu is sometimes blurred (Figs. 3(c−e)), according to the data obtained in Refs. [14,18]. Cr and Cu distributions in the blurred layers are of gradient nature toward the center of the chromium particles (Fig. 3(c)).

Some small chromium particles look completely blurry, for example, the particle at the end of the scanning line A−B (inset in Fig. 3(c)). The average content of copper in it, according to energy dispersive X-ray (EDX) analysis, is about 48%−50%. A homogeneous mixture of such a composition in equilibrium conditions can only exist at temperature ≥1750 °C (Fig. 4). This mismatch can only be explained by the micro-heterogeneity of the areas under investigation. In Figs. 3(d, e), some block inclusions of chromium in α-Cu can be seen. Thus, the blurred areas without clearly expressed interphase boundary consist of a mechanical mixture of α-Cu+β-Cr ultrafine phases.

The phase blockiness (mosaicity) of the blurred structures registered by the BSE sensor was revealed by an ion etching additional to the mechanical one with Linda SEM Prep 2 (5 min at 10 kV with a beam of 8 mm × 8 mm at an angle of 7°) (Figs. 3(d−f)). The image of the alloy surface after its etching also shows in secondary electrons its relief blockiness (inset in Fig. 3(f)).

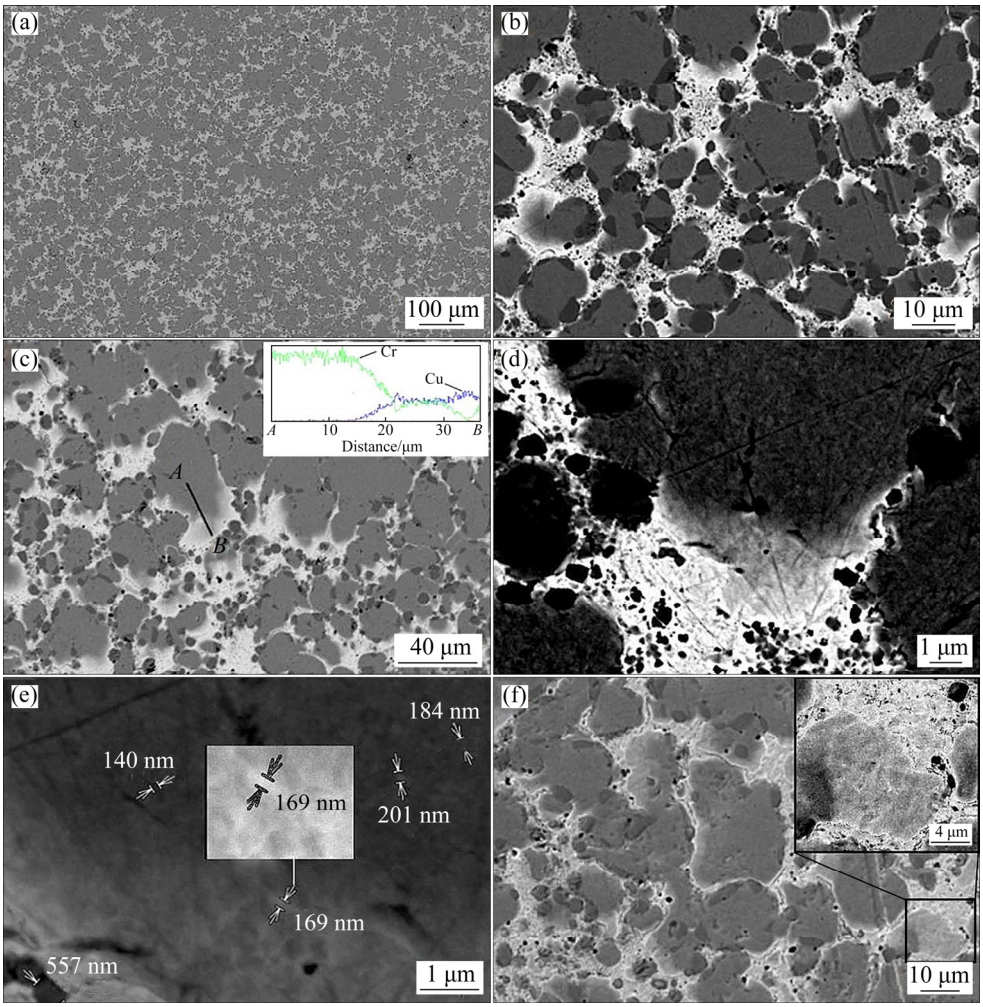

Fig. 3 Back-scattering electron (BSE) SEM images of microstructure of $Cr_{65}Cu_{35}$ alloy before arc-resistance tests: (a) General view of composite layer; (b, c) Morphologies of Cr grains (gray) and Cr_2N_{1-x} particles (black-gray), and EDX profile along *A*−*B* line; (d−f) Illustration of microheterogeneity and sizes of blocks in blurred Cr regions

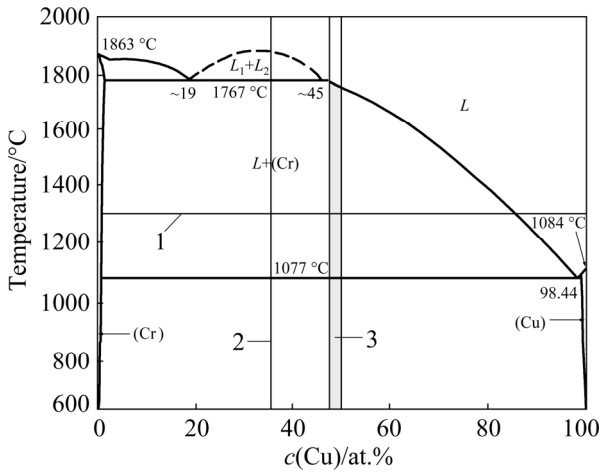

Fig. 4 Binary phase diagram of Cr−Cu system (redrawn according to Ref. [34]): 1−Temperature of alloy smelting; 2−Composition of $Cr_{65}Cu_{35}$ alloy; 3−Composition of blurred regions of α-Cu+β-Cr ultrafine mixtures in Fig. 3(c)

The copper matrix (according to SEM) except for the blurred α-Cu+β-Cr areas is also filled with ultrafine chromium inclusions of the secondary generation chromium (Cr^{Sec}) ("Sec" means the phases of the secondary and higher generations) and chromium nitrides Cr_2N_{1-x} (gray and black-gray phases, respectively) (see Figs. 3(b−e)). The reason for the Cr_2N_{1-x} originating in the alloy is the nitrogen in the air, which was adsorbed by the initial chromium powder particles and was not removed during alloy production [42]. The phases filling the matrix increase its microhardness to (1250±70) MPa.

The impact of the electric arc on the alloy leads to significant changes in the structure of the surface layers of the contacts. The structure fragments with a maximum thickness of the accumulated layer are shown in Figs. 5(a, b). The

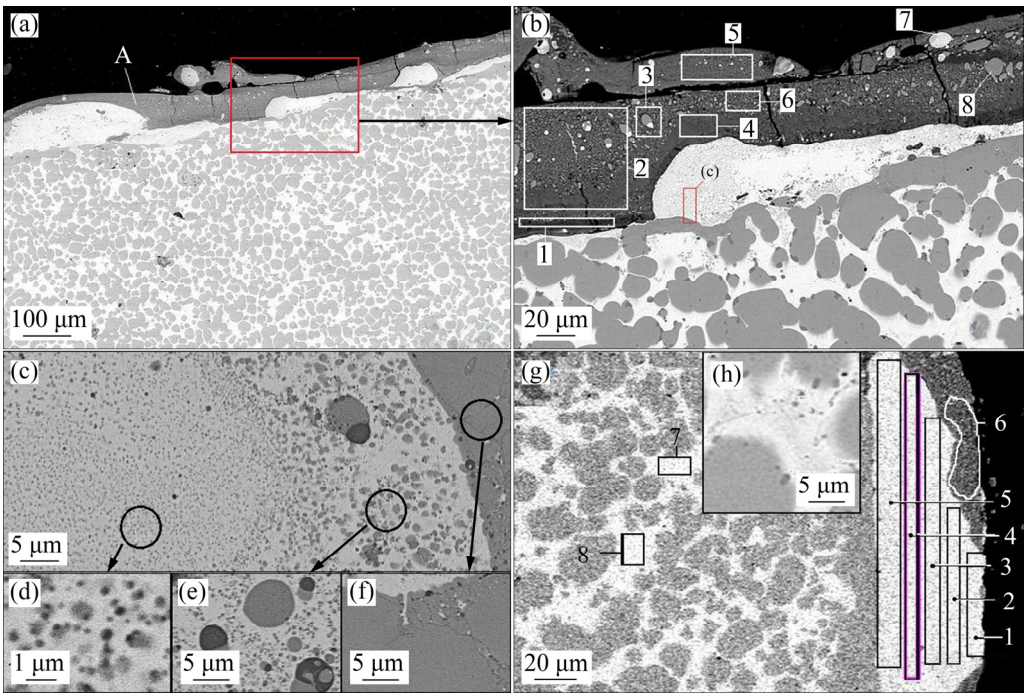

Fig. 5 Microstructures of $Cr_{65}Cu_{35}$ electrical contacts after arc-resistance test: (a) General view of upper layer contact; (b) Oxidized Layer A (Scanned areas are marked with numbers, and their compositions are given in Table 1); (c−f) Inclusions of Cr (gray) and Cr_2N_{1-x} (dark-gray) in unoxidized working layers; (g) Areas of EDX analysis of Cr content in unoxidized layers of lower contact; (h) Precursors of Cr dispersions

top layer is oxidized, with the compositions of oxidized layer given in Table 1. It has a dense composite-like structure with large vertical and horizontal cracks (Layer A). The thickness of Layer A is defined by the degree of peeling.

If contacts work in an oxygen-free atmosphere (for example, in a vacuum), the oxidized layer is not formed. In this regard, the structure of the non-oxidized working layer of the composite is of significant interest.

Table 1 Compositions of oxidized layer on $Cr_{65}Cu_{35}$ alloy surface after arc-resistance test

Scanned area in Fig. 5(b)	Composition/at.%				Cr/O	Cr/Cu
	Cu	Cr	O	N		
1	1	39	60	−	0.7	39
2	3	49	48	−	1.0	16.3
3	12	55	33	−	1.7	4.6
4	1	46	53	−	0.9	46
5	4	46	50	−	0.9	11.5
6	3	50	47	−	1.1	16.7
7	74	20	6	−	3.3	0.3
8	8	63	8	21	7.9	7.9

Analysis of the structure and composition of the unoxidized layers shows the strong saturation of α-Cu with ultrafine inclusions of chromium (Figs. 5(c−f)). The self-dispersion of chromium increases towards the contact surface along with an increase in temperature.

According to EDX microanalysis, the maximum content of Cr in the dispersion-strengthened sections of α-copper achieves 30%. Areas 2−5 in Fig. 5(g) contain 24.5−20.0 at.% Cr (Cu the rest). The gradual Cr decrease towards the contact surface is associated with the transition of Cr into an oxide. Thus, the Layer 6 in Fig. 5(g) contains $Cr_{49}Cu_3O_{48}$.

Uniform distribution of ultrafine and nanosized Cr particles and their morphology indicate overheating these areas of the contact above the liquidus line. Such high temperatures are entirely achievable when the contact surface is exposed to arc warming-up. Rapid cooling of the appeared homogeneous melt leads to the formation and subsequent disintegration of a supersaturated solid solution of Cu(Cr) (Fig. 4).

Below dispersed chromium (to the contact depth up to 200−400 μm), where the temperatures

are not so high, the aggregate of large grains of chromium and the matrix is filled with dispersions of Cr+α-Cu (Fig. 5(h)). The content of β-Cr in the latter depends on the distance to the surface (Spectrum 8: 3.1%, and Spectrum 7: 9.2% in Fig. 5(g)). This layer may be considered a precursor for the following stages of dispersion strengthening of α-Cu when the impact cycles of the arc are repeated.

Figure 5 shows that chromium self-dispersion taking place during the operation does not depend on the size of the initial chromium particles, which fall into the area of arc impact. Smooth relief of contacting surfaces is formed. Precipitation of Cr^{Sec} out of α-Cu provides strengthening without a significant decrease in electric conductivity.

Thus, both the dispersion of the phase components of the commutating surfaces and the passivation of Cu-matrix due to more active chromium oxidation provide running $Cr_{65}Cu_{35}$ electric contacts with "smart response" to functional loads in the presence of oxygen as well as in an inert atmosphere.

3.2 $W_{45}Cu_{55}$ alloy

Using $W_{45}Cu_{55}$ alloys with different packing of W-phase (the frame packing in Alloy 1, and the frameless one in Alloy 2), the difference is found in arc-resistance and structure evolution after the impact of an electric arc. External surfaces of the electrodes after arc-erosion tests are represented in Ref. [12].

Alloy 1 was produced by mechanically processing an industrial electrical contact with an average tungsten content of 45%. Its portion was up to about 75% within the top contact layer (width of 800−1000 μm). Alloy 2 was produced by the method described above in Section 2.2.

Figure 6 shows the microstructure of the alloys after the arc-resistance tests. The images show both the accumulated layers and the deeper layers with the unchanged initial structure.

The initial structure of Alloy 1 is a frame of tungsten layers, fully impregnated with copper. The layers of W are extended along the working surface of the contacts and have the length of 20−200 μm, and the width of 10−30 μm (Figs. 6(a, b)).

The initial structure of Alloy 2 is represented by inclusions of the dispersed (1−3 μm) particles of W in the Cu-matrix. The particles of W exist in the alloy as clusters of different sizes. The wide interlayers of copper between large clusters are also filled with dispersed inclusions of W or their small associates (Figs. 6(c, d)). All the tungsten particles

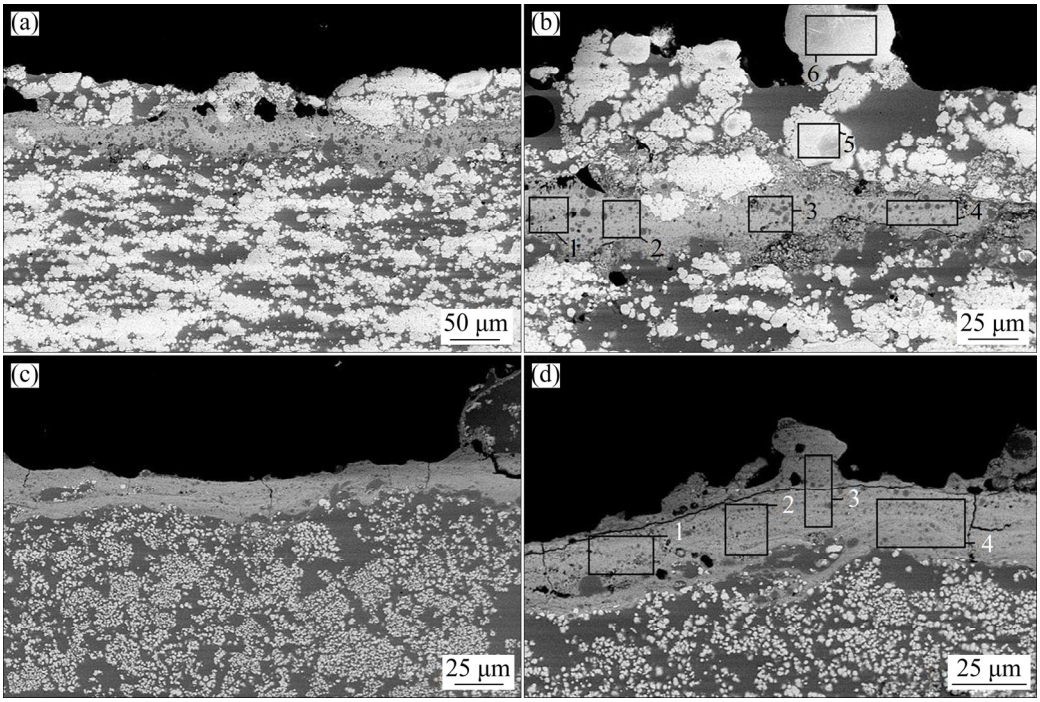

Fig. 6 Microstructures of surface layers of $W_{45}Cu_{55}$ electrical contacts made of Alloys 1 (a, b) and 2 (c, d) (Numbers indicate areas of EDX analysis)

in any cluster must be separated from each other with Cu-interlayer.

The average hardness values of Alloys 1 and 2 before the tests are (172±6) and (117±6) $HV_{5/15}$, respectively. The lower hardness of Alloy 2 is related to both the absence of a rigid W-frame and less content of W in the alloy surface layers.

The formation of tungsten clusters in Alloy 2 can be explained by the good cohesion and autohesion of tungsten particles in the initial powder. If conventional methods of powders admixing to liquid phase are used, their aggregates behave in a liquid flow like one big particle. When the liquid−solid mixture undergoes vibration, tungsten particles are separated by the liquid phase due to the intensification of capillary forces and mobility of individual particles inside the aggregates. Our conclusions are in good agreement with the data from other work [3], where the authors observed similar behavior of tungsten particles under high-frequency (600 Hz) treatment of bimodal tungsten powder in molten copper.

During arc-resistance tests, the accumulated layers gradually covered the surface area of the electrical contacts. The surface of Alloy 1 was completely oxidized after 3000 on/off cycles, and that of Alloy 2 was oxidized after 5000 cycles [12].

The comparison of the average composition of the structurally uniform oxidized layers of Alloys 1 and 2 (Areas 1−4 in Figs. 6(b, d)) is given in Table 2. It can be seen that the change of W content in Alloy 1 is almost an order of magnitude higher, although the total oxidation level of layers in the alloys does not differ greatly.

Table 2 Average compositions of homogeneously oxidized areas of $W_{45}Cu_{55}$ alloys

Alloy No.	Composition/at.%			W/Cu
	W	Cu	O	
1	33.5±8.5	17.0±2	61.5±3.5	2.0
2	22.0±1.0	21.0±4	57.0±4.5	1.0

The frame of W was gradually destroyed in the submelted layers of Alloy 1 under the influence of an arc. At the same time, both divisions of the frame into parts of different sizes (2−60 μm) and their fusion took place. Those processes led to the formation of the rough relief of the working surface. Figures 6(a, b) (EDX Areas 5 and 6) show that the big newly-formed particles consist of W. And the structure of the oxidized layer presents with W cores inside the mantle of W_xO_y. At the same time, in frameless Alloy 2, W particles do not sinter with each other at all, even in the top layers of the contacts where the arc creates enormous heat (Figs. 6(c, d)).

Thus, the advantages of Alloy 2 are the follows: initially more plastic general structure of the contact, more regular relief of the commuting surfaces, absence of rough W-inclusions both on the contact surfaces and in the unoxidized working area, higher homogeneity of the composition of the oxidized layers, and higher copper content in them (Table 2). We can argue that exactly those properties of Alloy 2 make it more arc-resistant despite of less content of W in it.

A frameless structure similar to that produced in this work is not often described in publications. In Ref. [9] such structure was produced by hot pressing in the vacuum of the mixture of tungsten (50 wt.%) and Al-alloyed copper powders. However, the reported synthesis of the alloy [9] took one order of magnitude more time than the method described in this work.

3.3 $W_{14}Cr_{32}Cu_{54}$ alloy

The above-described technique was used to synthesize $W_{14}Cr_{32}Cu_{54}$ alloy. The SEM−EDX method was used in three arbitrary selected areas (1, 2, and 12 mm^2) to determine the phase and chemical composition of the composite alloy. Microstructure and chemical composition data for the alloy are shown in Fig. 7(a). According to X-ray structural analysis, the alloy contains α-Cu, W, and (W,Cr) solid solutions based on the tungsten lattice. The ratio of W to Cr in $W_{14}Cr_{32}Cu_{54}$ alloy is marked on the binary W−Cr phase diagram (Fig. 8) [34].

The alloy synthesis was activated by applying low-frequency vibration to the compositions of "Cu melt−an uncompacted mixture of W and Cr powders". During the alloy production, the (W,Cr) solid solutions and a small amount of W^{Sec} were formed. All the refractory phases are separated with or permeated by copper interlayers.

Electric arc multiple impacts activated formation and destruction of the solid solutions $(W,Cr)^{Sec} \leftrightarrow (W)^{Sec} + (Cr)^{Sec}$. The content of W^{Sec} in

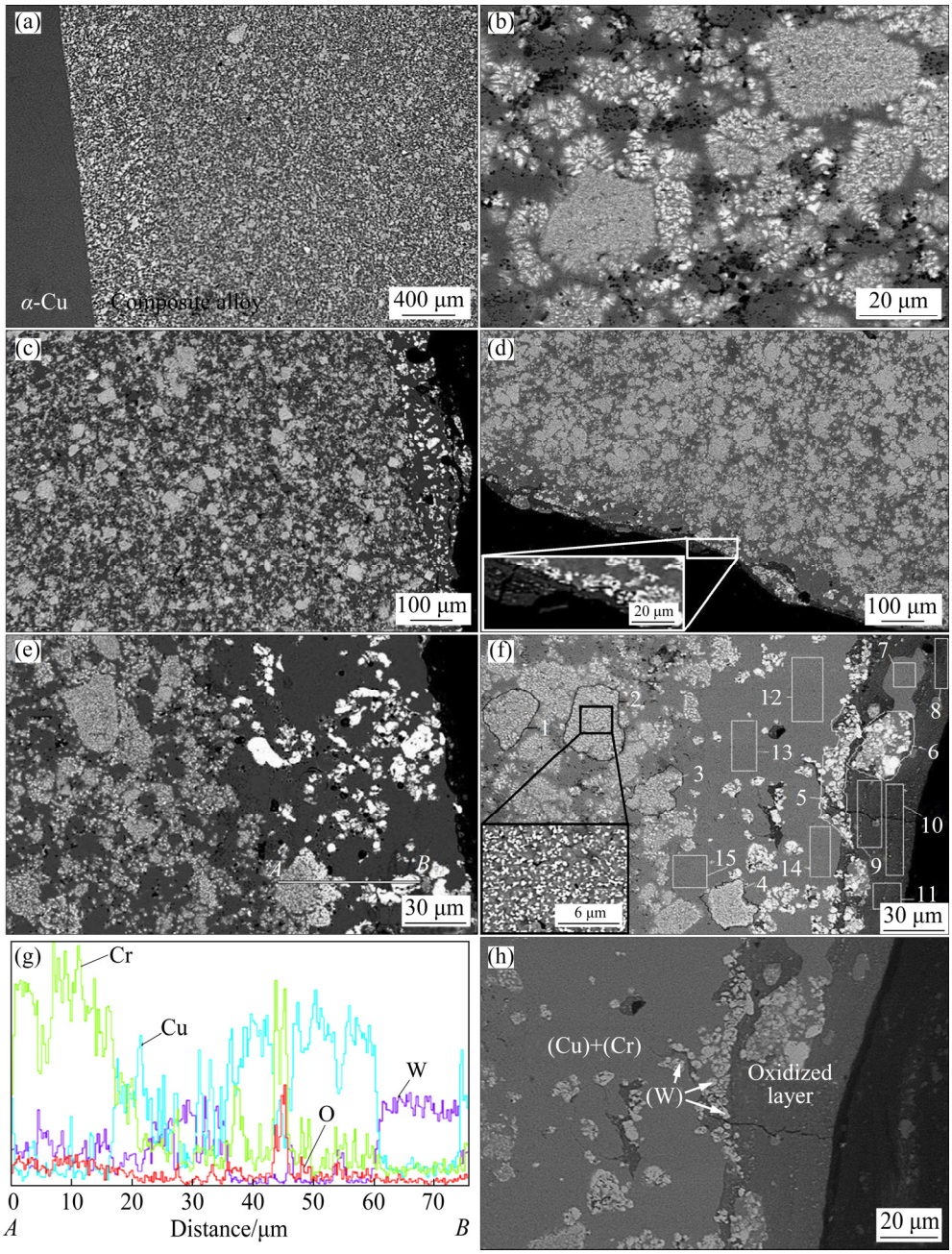

Fig. 7 Structures of $W_{14}Cr_{32}Cu_{54}$ alloys: (a) General view of microstructure; (b) (W,Cr) solid solutions in copper matrix; (c, e) Microstructure of upper layers of electrical contacts after arc-erosion tests; (d, f, h) Microstructure of bottom layers of electrical contacts after arc-erosion tests; (g) EDX results of scanning along *A*−*B* line in (e)

the structure was increased, and its morphology became more explicit (Fig. 7(b)). The maximum changes resulting from arc-erosion tests took place in the structure of the contact surface layers to a depth of about 200 μm (Figs. 7(c−h)).

During the tests, the thickness of the copper layer along the commuting surfaces of electrical contacts was increased, and the matrix composition was enriched with dispersed chromium from 5.9% to 21.0% (Areas 5, 6, 12−15 in Fig. 7(f), and Table 3). However, chromium particles as a separate phase in the copper matrix were not discovered by the SEM due to the sensitivity limit. Therefore, an increase of Cr amount took place just in the arc action area of small size. In the main undamaged part of the alloy (according to SEM−EDX), α-Cu contains less than 1.5% of dissolved Cr.

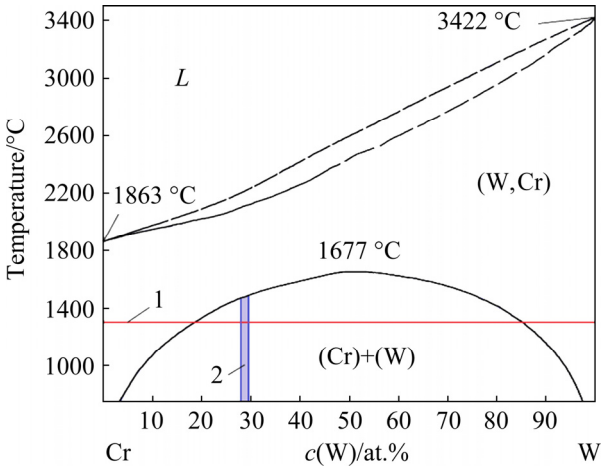

Fig. 8 Binary phase diagram of Cr−W system (reproduced from Ref. [34]): 1−Temperature of alloy smelting; 2−Ratio of W to Cr in $W_{14}Cr_{32}Cu_{54}$ alloy

The macro- and micro-segregation of W can be observed in the working layers of the contacts. The inclusions of W^{Sec} appeared both in $(W,Cr)^{Sec}$ aggregates and the working layer of the matrix. They are larger than those in the composite part (the white phase in Figs. 7(c−h)). The segregation of W is demonstrated by SEM images both for the upper and the bottom contacts. EDX analysis of the upper contact structure fragments was carried out along the *A*−*B* line with a length of 75 μm (Figs. 7(e, g)). The scanning line intersects the cluster of $(W,Cr)^{Sec}$, dispersed inclusions of W^{Sec}, *α*-Cu, and the product of macro-segregation (W^{Sec} inclusion) with an average diameter of about 10 μm.

Dispersed inclusions of W^{Sec} under the scanning line *A*−*B* demonstrate micro-segregation of W (Figs. 7(e, g)). The structure of a cluster $[(W,Cr)^{Sec}+W^{Sec}]$ is visible in Fig. 7(e). The inclusions of W^{Sec} (the white phase) cover the matrix of $(W,Cr)^{Sec}$ (the light grey phase) and interlayers of copper (the dark grey phase). It can be seen that the size of W^{Sec} and its general content in the cluster increase towards the contact surface. Macro- and micro-segregations of W^{Sec} are demonstrated in Fig. 7(g). The diagram shows two extrema of the tungsten content around 30 and 60 μm at the scanning line.

The unexpected result is that the vector of heavy particles W^{Sec} displacement is not associated with the gravitational force despite of the significant difference in the tungsten and copper densities. The segregation of W^{Sec} in the process of

Table 3 Compositions of structure fragments (Fig. 7(f)) of bottom contact working surface according to EDX analysis

Analyzed area	Composition/at.%				Cr/W	Structure fragment
	Cr	W	Cu	O		
1	59.5	21.9	18.6	−	2.7	Clusters of W^{Sec} in matrix [(W,Cr)+ *α*-Cu]
2	61.5	23.5	15.0	−	2.6	
3	59.4	20.0	20.6	−	3.0	
4	43.3	25.6	31.1	−	1.7	
5	13.3	29.2	57.5	−	0.46	Clusters of macro-segregations of W^{Sec} in *α*-Cu
6	21.0	19.0	20.4	39.6	1.1	
7	11.7	−	88.3	−	−	*α*-Cu in oxide layer
8	50.0	−	−	50.0	−	Homogeneous oxide layer
9	42.5	1.7	3.2	52.6	25.0	
10	45.8	0.8	−	53.4	57.3	
11	47.5	−	−	52.5	−	
12	7.5	−	92.5	−	−	*α*-Cu matrix enriched with dispersed chromium
13	7.7	−	92.3	−	−	
14	5.9	−	94.1	−	−	
15	11.5	−	88.5	−	−	
Initial alloy	32.0	14.2	53.8	−	2.25	Alloy average composition

periodical “submelting” of the alloy by the electric arc takes place in both the upper and the bottom contacts towards their surfaces.

It is quite logical to assume that the segregation of W is a consequence of the more intense dissociation (W,Cr)→(W)+(Cr) at elevated temperatures. This is also confirmed by the chromium migration to the working area of contact. The ratio of Cr to W in the clusters decreases from 2.7 to 0.46 as it gets closer to the surface (Areas 1−6 in Fig. 7(f), and Table 3) due to chromium oxidation. Meanwhile, it is important to note that the particles of the secondary W^{Sec} seldom fuse thanks to copper interlayers. A similar result was described for $W_{45}Cu_{55}$ frameless alloys.

The work of the contacts in the air leads to an oxide layer formed on the surfaces. The composition of the layer, according to EDX analysis (as well as in $Cr_{65}Cu_{35}$ alloy), mainly corresponds to chromium monoxide (Areas 8−11 in Fig. 7(f), and Table 3). The vertical and horizontal cracks in the layer provide peeling of the oxidized layers and refreshment of the working contact surface (inset in Fig. 7(d)).

The segregation of W ends with the complete decomposition of (W,Cr) at the border with the oxide layer. A “new covering layer” of the contact is formed here from electroconductive arc-resistant phase compositions in dispersion-strengthened copper. They contain more W and less Cr compared to the bulk of the initial composite alloy due to the migration of chromium into the oxide layer (Figs. 7(c−f), and Table 3). This allows the working contacts to have higher values of the hardness of the contact working layer while maintaining the plasticity.

The size of macro-segregated W in the “new covering layer” is larger than that in the frameless alloy $W_{45}Cu_{55}$ but smaller than that in the framed commercial alloy. Such fragments can also be seen inside the oxidized layer (Figs. 7(f, h)).

3.4 Oxidation of alloys

The comparison of oxidation for all three alloys is given in Table 4.

Table 4 shows that the content of copper in the oxidized layer decreases dramatically for complete substitution of W in the alloy with Cr and for its partial replacement. The contents of oxidized tungsten in $W_{14}Cr_{32}Cu_{54}$ alloy, compared to $W_{45}Cu_{55}$, decreased to 1.3 at.%. The latter confirms the well-known effect of tungsten passivation due to chromium additions [20−23].

Table 4 Average compositions of homogeneously oxidized areas of contacts

Composition of initial alloy	Composition of oxidized areas/at.%			
	W	Cr	O	Cu
$W_{45}Cu_{55}$	22.0	−	57.0	21.0
$Cr_{65}Cu_{35}$	−	48.0	47.8	4.2
$W_{14}Cr_{32}Cu_{54}$	1.3	46.5	52.2	0.8

Such changes indicate the synergetic effect of chromium influence on the protection of tungsten and copper against oxidation. The findings show that apart from Cr content, its source plays an important part (chromium as an initial component or as the product of (W,Cr) solid solution dissociation).

Thus, the structural changes of the working layers of $W_{14}Cr_{32}Cu_{54}$ alloys under the influence of an electric arc combine the similar changes in $Cr_{65}Cu_{35}$ and $W_{45}Cu_{55}$ alloys but are more efficient due to periodic dissociation−synthesis of (W,Cr) solid solutions.

4 Conclusions

(1) The “smart response” of the structure of $Cr_{65}Cu_{35}$ and $Cr_{32}W_{14}Cu_{54}$ electrical contacts to repeated exposure to an electric arc is manifested in the self-passivation of W and Cu with chromium via the self-dispersion of phase components by different mechanisms. An increase in the arc resistance of contacts is shown when changing the frame packing of W to frameless when using, as an example, the $W_{45}Cu_{55}$ alloy.

(2) Chromium, a decomposition product of a solid solution (W,Cr), passivates W and Cu more actively than an individual additive to copper.

(3) The evolution of the structure of Cr−W−Cu alloys under repeated periodic exposure to high temperatures indicates the prospects of their use as various materials operating under similar conditions. This suggests the need for further study.

Acknowledgments

The work was carried out within the State Assignment framework of IMET UB RAS using the equipment of the "Ural-M" Center for collective use. The authors are grateful to our colleagues Dr. O. M. FEDOROVA, Dr. L. A. OVCHINNIKOVA, Dr. A. S. BYKOV, Mrs. L. A. MARSHUK, Mr. I. S. SIPATOV, and Mr. O. A. KOROLEV for their help in doing this research.

References

[1] SLADE P G. The vacuum interrupter: Theory, design, and application [M]. Boca Raton: CRC Press, 2008.

[2] MIAO Bai-he, ZHANG Yan, LIU Guo-xun. Current status and developing trends of Cu−Cr manufacturing technique contact materials for VCB [C]// Proc of XXIst International Symposium on Discharges and Electrical Insulation in Vacuum. Yalta, Crimea: IEEE, 2004: 311−314. DOI: 10.1109/DEIV.2004.1422608.

[3] JANKOVIC ILIC D, FISCINA J, GONZALEZ O C, ILIC N, MÜCKLICH F. Self formed Cu−W functionally graded material produced via powder segregation [J]. Advanced Engineering Materials, 2007, 9(7): 542−546. DOI: 10.1002/adem.200700095.

[4] FAN Zhi-kang, LIANG Shu-hua, XUE Xu. Bond strength of W−Cu/CuCr integrated material [J]. Transactions of Nonferrous Metals Society of China, 2001, 11(6): 835−837.

[5] ZHOU Cheng-shang, LI Li-ya, WANG Jia, YI Jian-hong, PENG Yuan-dong. A novel approach for fabrication of functionally graded W/Cu composites via microwave processing [J]. Journal of Alloys and Compounds, 2018, 743: 383−387. DOI: https://doi.org/10.1016/j.jallcom.2018.01.372.

[6] DONG Long-long, CHEN Wen-ge, HOU Lin-tao, DENG Nan, ZHENG Cheng-hao. W−Cu system: synthesis, modification, and applications [J]. Powder Metallurgy and Metal Ceramics, 2017, 56(3−4): 171−184. DOI: 10.1007/s11106-017-9884-6.

[7] DONG L L, AHANGARKANI M, CHEN W G, ZHANG Y S. Recent progress in development of tungsten−copper composites: Fabrication, modification and applications [J]. International Journal of Refractory Metals and Hard Materials, 2018, 75: 30−42. DOI: doi.org/10.1016/j.ijrmhm.2018.03.014.

[8] CHEN Xiang, LI Xiao-jie, YAN Hong-hao, WANG Xiao-hong, MIAO Yu-song. Explosive compact-coating of tungsten–copper alloy to a copper surface [J]. Materials Research Express, 2017, 4(3): 036502. DOI: https://doi.org/10.1088/2053-1591/aa664c.

[9] TIAN B H, ZHANG X W, ZHAO R L, LIU Y, JIA S G, REN F Z. Microstructure and properties of vacuum hot-press sintered W/Cu−Al_2O_3 composite [J]. Reviews on Advanced Materials Science, 2013, 33(3): 219−223.

[10] HE Wen-xiong, YU Yang, WANG Er-de, SUN Hong-fei, HU Lian-xi, CHEN Hui. Microstructures and properties of cold drawn and annealed submicron crystalline Cu−5%Cr alloy [J]. Transactions of Nonferrous Metals Society of China, 2009, 19: 93−98. DOI: 10.1016/S1003-6326(08)60234-4.

[11] XIU Shi-xin, YANG Ren, XUE Jun, WANG Jin-xing, WANG Jia-yi. Microstructure and properties of CuCr contact materials with different Cr content [J]. Transactions of Nonferrous Metals Society of China, 2011, 21: 389−393.

[12] BODROVA L E, MELCHAKOV S Yu, GOYDA E Yu, SHUBIN A B. Synthesis of arc-resistant W70Cu30 composite alloy with frameless placing of thin-dispersed tungsten phase [J]. Inorganic Materials: Applied Research, 2020, 11(2): 495−502. DOI: 10.1134/S2075113320020070.

[13] ZHAO Qing, SHAO Zhong-bao, LIU Cheng-jun, JIANG Mao-fa, LI Xue-tian, ZEVENHOVEN R, SAXEN H. Preparation of Cu−Cr alloy powder by mechanical alloying [J]. Journal of Alloys and Compounds, 2014, 607: 118−124. DOI: http://dx.doi.org/10.1016/j.jallcom.2014.04.054.

[14] CHAI Lin-jiang, ZHOU Zhi-ming, XIAO Zhi-pei, TU Jian, WANG Ya-ping, HUANG Wei-jiu. Evolution of surface microstructure of Cu−50Cr alloy treated by high current pulsed electron beam [J]. Science China Technological Sciences, 2015, 58(3): 462−469. DOI: 10.1007/s11431-015-5774-7.

[15] CHANG S H, LIANG C, HUANG J R, HUANG K T. Cr50Cu50 alloys produced from submicrometre structured powders through hot pressing at different pressures [J]. Powder Metallurgy, 2016, 59(2): 142−147. DOI: 10.1080/00325899.2015.1132033.

[16] ZHANG Cheng-yu, YANG Zhi-mao, WANG Ya-ping, DING Bing-jun, GUO Yong. Preparation of CuCr25 contact materials by vacuum induction melting [J]. Journal of Materials Processing Technology, 2006, 178: 283−286. DOI: 10.1016/j.jmatprotec.2006.04.010.

[17] BRAUNOVIC M, KONCHITS V V, MYSHKIN N K. Electrical contacts: Fundamentals, application and technology [M]. Boca Raton: CRC Press, 2007. DOI: https://doi.org/10.1201/9780849391088.

[18] BODROVA L E, MELCHAKOV S Yu, SHUBIN A B, GOIDA E Yu, MARSHUK L A. Synthesis of Cu−Cr composite alloys with a layered structure featuring high arc resistance [J]. Inorganic Materials: Applied Research, 2019, 10(5): 1129−1134. DOI: 10.1134/S2075113319050034.

[19] BODROVA L E, PASTUKHOV E A, OVCHINNIKOVA L A, GOYDA E Yu. Formation of finely dispersed structure of W during the liquid-phase of obtaining of composite alloys Cu−10%Cr−10%W through vibration [J]. Tsvetnye Metally, 2018, 2: 64−69. DOI: 10.17580/tsm.2018.02.08. (in Russian).

[20] VILEMOVA M, ILLKOVA K, LUKAC F, MATEJICEK J, KLECKA J, LEITNER J. Microstructure and phase stability of W−Cr alloy prepared by spark plasma sintering [J]. Fusion Engineering and Design, 2018, 127: 173−178. DOI: doi.org/10.1016/j.fusengdes.2018.01.012.

[21] WEISSGAERBER T, KLOEDEN B, KIEBACK B. Self-passivating tungsten alloys [C]//Proc Powder

Metallurgy World Congress & Exhibition. Florence, Italy, 2010, 3: 377−383.

[22] CALVO A, GARCIA-ROSALES C, KOCH F, ORDAS N, ITURRIZA I, GREUNER H, PINTSUK G, SARBU C. Manufacturing and testing of self-passivating tungsten alloys of different composition [J]. Nuclear Materials and Energy, 2016, 9: 422−429. DOI: http://dx.doi.org/10.1016/j.nme.2016.06.002.

[23] WEGENER T, KLEIN F, LITNOVSKY A, RASINSKI M, BRINKMANN J, KOCH F, LINSMEIER Ch. Development and analyses of self-passivating tungsten alloys for DEMO accidental conditions [J]. Fusion Engineering and Design, 2017, 124: 183−186. DOI: http://dx.doi.org/10.1016/j.fusengdes.2017.03.072.

[24] KOCH F, BOLT H. Self passivating W-based alloys as plasma facing material for nuclear fusion [J]. Physica Scripta, 2007, T128: 100−105. DOI:10.1088/0031-8949/2007/T128/020.

[25] GARCIA-ROSALES C, LOPEZ-RUIZ P, ALVAREZ-MARTIN S, CALVO A, ORDAS N, KOCH F, BRINKMANN J. Oxidation behaviour of bulk W−Cr−Ti alloys prepared by mechanical alloying and HIPing [J]. Fusion Engineering and Design, 2014, 89: 1611−1616. DOI: http://dx.doi.org/10.1016/j.fusengdes.2014.04.057.

[26] KOCH F, BRINKMANN J, LINDIG S, MISHRA T P, LINSMEIER Ch. Oxidation behaviour of silicon-free tungsten alloys for use as the first wall material [J]. Physica Scripta, 2011, T145: 014019. DOI: doi:10.1088/0031-8949/2011/T145/014019.

[27] CALVO A, GARCIA-ROSALES C, ORDAS N, ITURRIZA I, SCHLUETER K, KOCH F, PINTSUK G, TEJADO E, PASTOR J Y. Self-passivating W−Cr−Y alloys: Characterization and testing [J]. Fusion Engineering and Design, 2017, 124: 1118−1121. DOI: http://dx.doi.org/10.1016/j.fusengdes.2017.03.001.

[28] CALVO A, SCHLUETER K, TEJADO E, PINTSUK G, ORDAS N, ITURRIZA I, NEU R, PASTOR J Y, GARCIA-ROSALES C. Self-passivating tungsten alloys of the system W−Cr−Y for high temperature applications [J]. International Journal of Refractory Metals & Hard Materials, 2018, 73: 29−37. DOI: http://doi.org/10.1016/j.ijrmhm.2018.01.018.

[29] WEGENER T, KLEIN F, LITNOVSKY A, RASINSKI M, BRINKMANN J, KOCH F, LINSMEIER Ch. Development of yttrium-containing self-passivating tungsten alloys for future fusion power plants [J]. Nuclear Materials and Energy, 2016, 9: 394−398. DOI: http://dx.doi.org/10.1016/j.nme.2016.07.011.

[30] LITNOVSKY A, WEGENER T, KLEIN F, LINSMEIER Ch, RASINSKI M, KRETER A, TAN X, SCHMITZ J, MAO Y, COENEN J W, BRAM M, GONZALEZ-JULIAN J. Advanced smart tungsten alloys for a future fusion power plant [J]. Plasma Physics and Controlled Fusion, 2017, 59: 064003. DOI: http://doi.org/10.1088/1361-6587/aa6948.

[31] SCHMITZ J, LITNOVSKY A, KLEIN F, WEGENER T, TAN X Y, RASINSKI M, MUTZKE A, HANSEN P, KRETER A, POSPIESZCZYK A, MÖLLER S, COENEN J W, LINSMEIER Ch, BREUER U, GONZALEZ-JULIAN J, BRAM M. WCrY smart alloys as advanced plasma-facing materials – Exposure to steady-state pure deuterium plasmas in PSI-2 [J]. Nuclear Materials and Energy, 2018, 15: 220−225. DOI: doi.org/10.1016/j.nme.2018.05.002.

[32] TELU S, MITRA R, PABI Sh K. High temperature oxidation behavior of W−Cr−Nb Alloys in the temperature range of 800−1200 °C [J]. International Journal of Refractory Metals and Hard Materials, 2013, 38: 47−59. DOI: http://dx.doi.org/10.1016/j.ijrmhm.2012.12.008.

[33] TELU S, MITRA R, PABI Sh K. Effect of Y_2O_3 addition on oxidation behavior of W−Cr alloys [J]. Metallurgical and Materials Transactions A, 2015, 46: 5909−5919. DOI: 10.1007/s11661-015-3166-z.

[34] LYAKISHEV N P. Binary alloy phase diagrams: Handbook [M]. Vol. 2. Moscow: Mashinostroenie, 1997. (in Russian)

[35] IGNAT'EV I, PASTUKHOV E, BODROVA L. Method for alloys obtained by low-frequency treatment of their melts [M]. Saarbrucken: LAP LAMBERT Academic Publishing, 2013. (in Russian).

[36] BODROVA L E, PASTUKHOV E A. Interaction between vanadium carbide and aluminum and copper melts [J]. Russian Metallurgy (Metally), 2013(2): 112−114. DOI: 10.1134/S0036029513020055.

[37] BODROVA L E, GOIDA E Yu, PASTUKHOV E A, MARSHUK L A, POPOVA E A. Interaction of tungsten with tungsten carbide in a copper melt [J]. Russian Metallurgy (Metally), 2013(7): 491−496. DOI: 10.1134/S0036029513070033.

[38] IGNAT'EV I E, PASTUKHOV E A, BODROVA L E, IGNAT'EVA E V, GOIDA E Yu. Features of the low-frequency treatment of melts [J]. Russian Journal of Non-Ferrous Metals, 2013, 54(3): 215−219. DOI: 10.3103/S1067821213030073.

[39] BODROVA L E, PASTUKHOV E A, GOIDA E Yu, OVCHINNIKOVA L A. Synthesis of cast graphite-containing Cu–Cr–C composites [J]. Russian Metallurgy (Metally), 2017(1): 67–73. DOI: 10.1134/S0036029517010025.

[40] BODROVA L E, FEDOROVA O M, SHUBIN A B, PASTUKHOV E A. Interaction of niobium and tungsten monocarbides in molten copper [J]. Russian Metallurgy (Metally), 2017(3): 204−208. DOI: 10.1134/S0036029517030003X.

[41] BODROVA L E, GOIDA E Yu, PASTUKHOV E A, CHENTSOV V P. Optimization of liquid-phase method of synthesis of Cu−W alloys [J]. Inorganic Materials: Applied Research, 2018, 9(2): 311−316. DOI: 10.1134/S2075113318020053.

[42] MELCHAKOV S Yu, BODROVA L E, GOYDA E Yu, SHUBIN A B, SOMOV P A. Experimental production of Cu–Cr–N composite alloys and thermodynamic modeling of their phase composition [J]. Inorganic Materials: Applied Research, 2019, 10(6): 1357−1364. DOI: 10.1134/S2075113319060145.

铜中无骨架填充 Cr 和 W 电触头复合材料的智能显微组织

L. E. BODROVA, S. Yu. MELCHAKOV, A. B. SHUBIN, E. Yu. GOYDA

Institute of Metallurgy of the Ural Branch of the Russian Academy of Sciences,
620016, Ekaterinburg, 101, Amundsen Street, Russian Federation

摘　要：为了研究抗电弧断路器合金显微组织的智能响应机制，制备 $W_{45}Cu_{55}$、$Cr_{65}Cu_{35}$ 和 $Cr_{32}W_{14}Cu_{54}$ 合金。与工业合金不同，这些合金中 Cr 和 W 相是无骨架填充到铜基体中。其制备方法是在振动(80 Hz)下，将铜熔体渗透到未压实的 Cr 和 W 混合粉末中。结果显示，当 W 由“骨架”填充变为“无骨架”填充后，触头的抗弧性能有所提高，Cr 对抗弧相的自扩散和 W、Cu 钝化过程起决定性作用。基于所得结果，总结铜中无骨架填充抗电弧相的优点，以及含 Cr 触头显微组织在含氧和惰性气氛下对功能载荷响应时“智能行为”的原因。

关键词：Cr−W−Cu 电触头材料；熔渗；智能结构；自扩散

(Edited by Bing YANG)